Applied Surface Science Advances 7 (2022) 100194

Contents lists available at ScienceDirect

Applied Surface Science Advances

journal homepage: www.sciencedirect.com/journal/applied-surface-science-advances

Sliding on snow of Aisi 301 stainless steel surfaces treated with ultra-short laser pulses

Ettore Maggiore [a], Inam Mirza [b], David Dellasega [c], Matteo Tommasini [a], Paolo M. Ossi [c,*]

[a] Dipartimento di Chimica, Materiali e Ingegneria Chimica "G. Natta", Politecnico di Milano, 20133 Milano, Italy
[b] HiLASE Center, Institute of Physics of the Czech Academy of Sciences (CAS), Za Radnici 828, Dolní Břežany, 252 41, Czech Republic
[c] Dipartimento di Energia, Politecnico di Milano, 20133 Milano, Italy

ARTICLE INFO

Keywords:
AISI 301
Surface engineering
LIPSS
Hydrophobic surface
Snow
Friction

ABSTRACT

Surface irradiation of AISI 301 with ultra-short linearly polarized pulses between 247 fs and 7 ps resulted in laser induced periodic surface structures (LIPSS). Scanning electron microscope micrographs taken after the laser treatment show the formation of sub-micrometer sized arrays of nearly parallel ripples slightly differing from each other, depending on the specific treatment adopted. Static contact angle data indicate that LIPSS induce a marked hydrophobic behavior of the treated surfaces. The friction coefficient of laser treated and pristine AISI 301 surfaces gliding on compact snow was compared to that of ultra-high molecular weight polyethylene. The friction coefficients of the laser treated samples are intermediate between those of bare AISI 301 and of UHMWPE. The changes in contact angle and surface morphology of the samples after extensive tribometer tests were tested to investigate the durability of LIPSS.

1. Introduction

Top-level sport tools are the ideal frame to explore advanced technology-based innovation. In the case of alpine ski, the skis are to be easy to maneuver, allowing rapid and controlled changes of direction and velocity, they must be torsionally rigid, they have to show consistent longitudinal bending stiffness so as to efficiently absorb the vibrations caused by the terrain and snow irregularities, they have to glide fast on snow with markedly different characteristics. As an additional likely feature they should be as light as possible. Looking back at the history of alpine skiing competitions, a parallel trend is evident in the evolution of the ski structure and lateral shaping (side cut), the skiing technique, the slope design and preparation. Sharp and polished ski edges allow for keeping and maintaining a precise trajectory; gliding on snow is facilitated by the low friction coefficient of the ski bases. The latter can be further reduced by proper waxing. Quite curiously, both ski edges and ski bases did not significantly improve since the introduction in the early 1970's of ultra-high molecular weight polyethylene (UHMWPE; MW, 13 $\times$ 10^6 Da) and low carbon steel, like C60 with good wear and abrasion resistance, superior toughness for impact damage, acceptable ductility. The reason is twofold: (i) on *natural* snow UHMWPE (both sintered or extruded and added with graphite or silicon particles to improve its thermal and electrical conductivity allows for fast sliding; (ii) C60 (edges) allows an easy and precise trajectory control. Noticeably, both materials are rather economic and easy to manufacture. In particular, the surface of an UHMWPE foil (initial thickness 1.5 mm) in contact with snow is subjected to grinding: specific machines exploit a hard stone to apply by abrasion the desired surface pattern to such a ski base. The process reduces friction, decreasing the capillary force between the base and snow [1], efficiently and quickly removing the meltwater film produced by frictional heating at the base-snow contact surface [2]. Natural, freshly deposited snow is a loosely packed granular material made of coexisting ice micro-crystals, a fraction of liquid water and water vapor. Snow undergoes spontaneous, extensive metamorphism since its deposition: thus, progressively accumulated seasonal layers that constitute the snowpack show very different grain size, compactness and hardness, resulting from the combined effect of temperature, relative humidity, wind, as the main factors. Snow friction was reviewed in [3] and ice friction was studied in [4]. Specific attention was paid to the role of surface roughness, structure, and hydrophobicity [5]. In the case of metallic surfaces, the efficiency of laser treatments including laser texturing and direct laser interference was investigated [6,7,8]. Competitive ski is normally performed on slopes prepared with artificial snow. The latter is the output of a kinetically accelerated process that

* Corresponding author.
E-mail address: paolo.ossi@polimi.it (P.M. Ossi).

https://doi.org/10.1016/j.apsadv.2021.100194
Received 20 July 2021; Received in revised form 17 November 2021; Accepted 17 November 2021

mimics a natural snowfall and produces spheroidal micrometer-sized grains of hexagonal ice, I_h. The latter are accumulated on the ground, then properly distributed and compacted on the slope, thanks to powerful snowcats. For high level competitions, deliberate water injection in the compacted snow is performed to guarantee that the slope conditions are kept virtually unaltered even after many athletes skied on nearly the same trajectory along a sequence of gates. This means that ski edges and bases interact with highly compressed, very compact snow rather different from natural snow. As a consequence of extensive wear, irreversible damage of both components is often observed, even after one single timed run. In recreational skiing, although less dramatic, the limits of traditional materials for bases and edges again emerge after skiing for a moderate number of times on slopes prepared with artificial snow. Since the required maintenance is costly and time consuming, often the recreational skier does not keep in proper conditions his skis and finds ever growing difficulties to keep the desired trajectory and velocity, while the quality of the edges and bases progressively gets worse. Correspondingly increases the risk of injuries associated to a collision with an obstacle, or to a fall on the slope. Focusing on the ski bases, we made attempts at modifying, or synthesizing *carbon-based* materials with the aim to circumvent the above discussed intrinsic limitations of UHMWPE. We adopted strategies that involve laser technologies, such as laser irradiation of graphite [9], the synthesis of hard t-a C films [10], or of glass-like cluster assembled films [11], up to the deposition of DLC on polycarbonate [12]. Although exploratory, being still limited to the laboratory stage, the above studies did not provide robust indications that an increased resistance against wear and abrasion could be gained while keeping a gliding performance on snow comparable or at least not severely reduced with respect to that of UHMWPE (results subjected to Confidentiality Agreement).

To overcome the above issues, we explored metallic alloys as candidates for ski bases in a laboratory study on the friction behavior of the Titanal Al alloy and the AISI 301 stainless steel on different kinds of snow. We proposed a laser surface texturing treatment to produce a spatially homogeneous, equally spaced, dimple patterning (DP) of the metal surface with a control via laser parameters of the dimple geometry [13]. We observed [13] that DP resulted in hydrophobic behavior of both alloys, but it did not produce meaningful improvements in their gliding performance on snow at low and mid-low gliding velocities as compared to UHMWPE. Besides this, DP resulted in a modest performance deterioration with respect to untreated surfaces.

The friction coefficient of samples of Titanal and AISI 301, both pristine and subjected to DP, was measured with a custom-built snow tribometer in a climatic chamber, using packed, nearly icy snow, similar to the kind of snow experienced in high level competitions, at sliding velocities up to about 15 ms^{-1}. The gliding performance of both alloys at low and mid-low velocities was worse than that of UHMWPE, grinded and waxed state of the art, taken as the reference presently best performing ski base [13]. At high gliding velocities, above 15 ms^{-1} the friction coefficient of DP-modified Titanal was equal to that of UHMWPE (about 0.08) while that of AISI 301 was still higher by about 18% (about 0.098) [13].

Extensive testing [14] of prototype full-scale skis equipped with Titanal and AISI 301 ski bases (not surface treated), on slopes prepared with artificial snow for recreational skiing, showed that Titanal undergoes fast damage, being considerably softer than AISI 301 (hardness 2 GPa against 6 GPa, respectively). Consistently, after the tests, only shallow scratches were visible at the optical microscope on the surface of AISI 301. Thus, we focused on AISI 301 and we first reproduced on the steel base of a full size prototype ski and on tribometer samples the same stone grinding used for UHMWPE bases, using modified, hard SiC stones. Although apparently showing the same quality of macroscopic surface finishing, on every kind of snow, up to gliding velocities of 11 ms^{-1}, the performance of grinded AISI 301 was significantly worse than that of UHMWPE and of bare AISI 301 both waxed and non-waxed.

Further testing of prototype skis with the same geometry (length, sidecut) required for international competitions, equipped with *bare* AISI 301 bases, confirmed that at high speed such bases perform better than UHMWPE (artificial, highly compacted snow, timed runs, 25 gates, giant slalom and super-giant slalom courses; data subjected to Confidentiality Agreement). However, at low gliding speed, during the initial acceleration all the testers (top athletes) were unsatisfied with the performance of the steel bases.

We therefore explored surface treatments different to DP to improve the gliding performance of such a steel on snow.

Laser induced periodic surface structures (LIPSS) is an attractive, conceptually simple, easy to control surface patterning that can be produced on about any material once irradiated close to the macroscopic ablation threshold. LIPSS consists of a nearly periodic array of parallel lines that give rise to a surface relief the geometric parameters of which are closely correlated to the wavelength and the polarization of the incident laser radiation. Experiment shows that polarization strongly determines LIPSS orientation: for linear polarization a narrow set of regular thin lines defines the so called HSFL (High spatial frequency LIPSS), with spatial periodicity less than $\lambda/2$ (λ is the wavelength of the laser radiation) [15]. Further, another set of nearly periodic, mutually parallel ripples, with spatial periodicity larger than $\lambda/2$ defines the so called LSFL (Low spatial frequency LIPSS) [15]. With increasing laser intensity, within the Gaussian spot profile a transition from LSFL to grooves is observed. Two alternative models describe LIPSS formation. The first hinges on the idea of modulated ablation due to non-homogeneous energy deposition: the illumination pattern is attributed to the interference between the incident wave and surface plasmon-polaritons excited by the laser field itself [16,17]. In the second model, based on the ion sputtering analogue [18,19], the relaxation of the irradiated surface that is assumed to be a corrugated, thin liquid-like film involves the competition between the surface corrugation increase associated to desorption-induced surface roughening and the surface smoothing due to atomic diffusion [20].

Functional nano-structuring achieved by LIPSS formation was explored [15]. The modification of surface wettability of a stainless-steel surface to become superhydrophobic was reported [21] and the influence of LIPSS on the tribological properties of a treated steel surface was assessed [22].

Thus, we decided to adopt LIPSS, using fs and ps laser pulses, on AISI 301 samples suitable for test with our snow tribometer. We analyzed the produced surface morphology, we measured the contact angle with water droplets, and we performed friction coefficient measurements of the treated surfaces using highly compacted snow, so as to reproduce the conditions experienced by skis in a competition environment.

2. Experimental

To measure the sliding friction of surface modified AISI 301 on snow, we used 50 × 50 mm^2 samples cut from cold rolled sheets 0.5 mm thick (Lamina S.p.A., Milano, Italy).

For a realistic comparison we referred to a stone-grinded UHMWPE sample (1 mm thick) extracted from the central part of a competition (Super-giant slalom) ski base. Fig. 1 shows a picture of the typical UHMWPE surface morphology taken from our sample. The gliding direction is parallel to the grooves.

A commercial Yb:KGW laser system (PHAROS, Light Conversion) operating at a central wavelength of 1030 nm with fs to ps tunable pulse duration was used to irradiate the steel samples. Two AISI 301 samples (Hi-fs; Hi-ps) were irradiated with 247 fs and 7 ps pulses respectively. We made preliminary irradiations of a small AISI 301 1 × 1 mm^2 sample at varying fluence and overlap with the help of Galvano scanner. The diameter of the irradiation spot at $1/e^2$ of peak intensity on the sample surface (as measured using the method described in [23]) was 375 μm, as obtained placing the sample ~ 7 mm above the focal plane of Galvo lens. This way, for the same repetition rate, a more homogeneous and faster scanning of the sample area was possible without any polarization

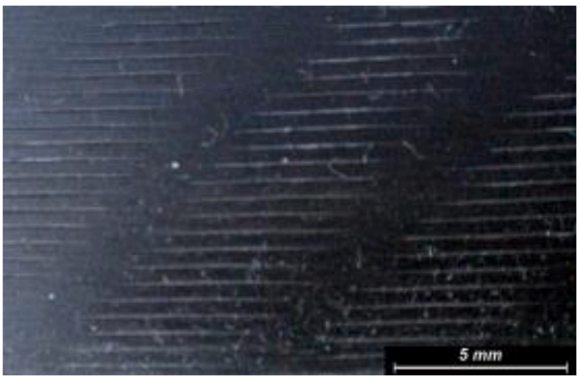

Figure 1. Stone-grinded reference UHMWPE ski base used for the tribometer tests.

deviation from linear behavior due to fast Galvo mirrors. In Galvano scanner, acceleration and deceleration phases of the beam are very short. As a result, the area of 1×1 mm^2 was structured pretty uniformly so that we could choose the laser parameters for the surface treatment of AISI 301 that are summarized in Table 1. Such laser parameters were selected starting from both SEM observation (presence and homogeneity of the LIPSS) and contact angle data. For both Hi-fs and Hi-ps samples, the laser parameters were: 0.94 W average power, 3 kHz laser repetition rate, 313 μJ energy per pulse and 0.57 Jcm^{-2} peak laser fluence. A combination of $\lambda/2$ wave plate and Glan-Taylor polarizer was used to reduce the maximum available pulse energy to the required value. For LIPSS formation on the whole sample area, both Hi-fs and Hi-ps samples were scanned under focused laser beam with the help of motorized, computer controlled XY scanning stages. The overlap between the $1/e^2$ spot diameter along the X-direction was adjusted to 75% by setting the scanning speed at 0.28 ms^{-1}. To adjust the same 75% overlap along the Y-direction, the distance between the scanning lines was set at 94 μm. To increase the laser processing speed, bi-directional scanning (left--right-left) was used. In these large samples, edge effects due to acceleration and deceleration of the motorized stage are present. However, such effects are negligibly small as compared to the overall scanned area of the sample. The effect of acceleration/deceleration of scanning at the edges of the scanned area was noticeable only within ~ 200 μm width where material ablation (slightly deeper surface relief) occurred, which however did not affect our measurements. In future applications the above effect can be excluded by scanning the sample with beam traces going beyond the sample area.

Two AISI 301 samples (LP-ps1; LP-ps2) were irradiated with 3 ps pulse duration at the wavelength of 1064 nm. The laser spot diameter on the sample surface was 100 μm, the average laser power 40 W, the repetition rate 500 kHz, the energy per pulse 80 μJ, the peak laser fluence 2.04 Jcm^{-2}. For both samples the overlap along the X-direction was 94% and that along the Y-direction was 15%.

We used a Zeiss Supra 40 field emission Scanning Electron Microscope (SEM), operating at an accelerating voltage of 5 kV to analyze the peculiarities of the LIPSS features produced on the irradiated samples. The Gwyddion software allowed us to calculate the average distance between the ripples on the sample surface.

To measure the friction coefficient of the samples on snow, we reproduced in the laboratory the sliding of a ski base on snow by using our custom-built snow tribometer (Fig. 2) [13]. The tribometer consists of a rotating aluminum annulus driven by a 250 W brushless electric motor connected to a controller that regulates the angular speed of the motor. Between two rails we inserted a carriage bearing the sample holder. We typically use an aluminum sample holder with a rounded front edge on which we attach the different samples with a double-sided tape. We inserted a steel bar and a cylindrical weight inside the carriage to press the sample holder on the snow surface. The steel bar is free to move in the vertical direction to follow the possible weak unevenness of the snow track during the sliding of the sample on snow.

We realized a removable Styrofoam support that fits inside the tribometer annulus to prepare and temporarily store the snow track inside a commercial freezer at controlled temperature. Before each test we cool down inside the freezer the sample attached to the sample holder so that they are at the same initial temperature as the snow surface.

The snow track is made of three compacted layers of different kinds of snow. For the bottom layer (5 mm thick) we used wet, natural snow (collected on field) with high water content. Inside the freezer we cooled down to –20°C such a snow layer converting it into ice. We prepared the intermediate snow layer by repeating the above procedure with the same snow supply. For the top layer (3 mm thick) we used laboratory-made snow [24], very similar to freshly deposited natural snow with small average grain size (~50 μm). Such a top layer provides a homogeneous spatial distribution of snow grains, and it allows to minimize the surface asperities of the track and the consequent vibrations of the slider. The snow track was initially kept at –1°C for 300 s so that the three layers could adhere well to each other, avoiding the possible detachment of the top layer caused by the shear force acting during the sample sliding. We remark that the preparation of the snow track is a critical procedure, since if the track is not accurately leveled, or if hard asperities are present on the surface, the vibrations of the slider (the amplitude of which increases with increasing sliding velocity) could progressively damage the snow track. If this occurs at elevated velocity (e.g. 10 ms^{-1} corresponding to 700 rpm [13]), the Styrofoam holder in particular is heavily stressed and it can catastrophically fail.

In a sliding test the slider travels along a "lane" centered on the center of the snow track. Before each sliding test, we tested and stabilized the snow track surface by sliding the UHMWPE sample at 4 ms^{-1} for a fixed time (120 s) to remove as far as possible residual small surface asperities.

We performed on each sample a series of five tests at maximum sliding speed of 7.2 ms^{-1} (low-speed tests), so as to operate the snow track in conditions reasonably far from the critical ones leading to track disruption. To keep reproducible testing conditions, we replaced the top layer after performing a series of tests on a given sample. To explore the sliding behavior at higher speeds, we performed *one single* test for each sample at a maximum speed of 9.4 ms^{-1} (high-speed tests). Indeed, at this speed it is difficult to repeatedly *and* affordably operate the tribometer because even a small imperfection of the snow surface causes

Table 1
Laser parameters adopted for the surface irradiation of AISI 301 (sample size 50 × 50 × 0.5 mm^3).

Sample	Power (W)	Pulse duration	Repetition rate	Pulse energy (μJ)
Hi-fs	0.94	247 fs	3 kHz	313
Hi-ps	0.94	7 ps	3 kHz	313
LP-ps1	40	3 ps	500 kHz	80
LP-ps2	40	3 ps	500 kHz	80

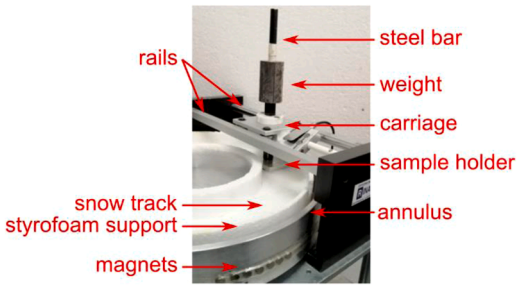

Figure 2. Snow tribometer with the Styrofoam container filled with snow inserted inside the aluminum annulus. The sample is held in place by the carriage, and it leans above the snow surface.

intense vibrations of the slider that progressively induce severe damage of the snow track.

We performed all the tribometer tests under ambient air conditioning at +15°C and relative humidity RH = 50%. For low-speed tests the initial temperature of the snow surface was –10°C, as measured before extracting the track from the freezer. Immediately after the end of each test (typical duration, 120 s since the track extraction from the freezer up to its re-insertion into the freezer) the measured surface temperature of the snow track increased to –5°C/–4°C. The same value of surface temperature of the snow track (–5°C/–4°C) was recorded at the end of the high-speed tests (duration, 180 s for the same cycling as for low-speed tests) that were started at a lower initial temperature of the snow surface (–15°C). In all tests the air temperature, recorded 3 mm above the track surface is constant at the value of 0.2°C, the RH being 14% along the entire test duration. Condensation of water vapor on the snow track surface can occur, yet the time required to the slider to travel at the *lowest* speed (1 ms^{-1}) one lap before passing a second time over a "lane" sector with its same length (50 mm) is 8.1×10^{-1} s. We take that this time is short enough to make irrelevant the condensation correction to μ value measurements. Just for a comparison with real conditions met during international competitions, we retrieved data from Italy National Winter Sports Federation (FISI), collected by official skimen along different 2021 World Cup downhill events in Europe (Kitzbuehl, Garmish Partenkirchen, Cortina d'Ampezzo). Values for snow temperature and RH, as well as air temperature and RH, taken at the same time and place, listed in the order, lie between (–23°C, 17%; –14.6°C, 21%) and (–1.6°C, 32%; +3.5°C, 89%). The evidence is that snow, although showing relevant temperature variations, has RH values much closed to each other, mostly centered around 25%, while air shows large variability both of temperature and of RH values. The role of water vapor condensation is much more relevant on a slope than in laboratory conditions.

To measure the angular speed (ω) of the snow track we mounted parallel to each other (180°) two neodymium magnets on the lateral external surface of the tribometer and we recorded as a function of time the number of rotations they performed with a Hall effect sensor (A3144).

2.1. Determination of the friction coefficient

To obtain the friction coefficient between the sample and snow, we recorded the angular velocity ω of the freely decelerating tribometer with the sample sliding on the snow track. After the desired maximum speed was reached, we turned off the motor and we immediately vertically moved the steel bar until the sample came into full contact with the snow track (Fig. 2). ω decreases because of the combined effect of the aerodynamic drag (AD) acting on the rotating surfaces, the mutual friction of the mechanical components (MF) and the friction between the sample and snow. Such three forces generate a torque that decelerates the tribometer until it stops. We can separately determine the AD and MF terms, collecting ω data as a function of time for the *slider-free* decelerating tribometer. The rotational energy depends on the inertia of the system around the rotation axis (I_z). For the tribometer loaded with snow we obtained $I_z = 0.2$ kg m^2 [25].

The rotational energy as a function of ω is given by

$$E(\omega) = \frac{I_z}{2}\omega^2 \tag{1}$$

and the dissipated power due to all the friction forces acting on the rotating tribometer is the time derivative of E(ω):

$$P = \frac{dE}{dt} \tag{2}$$

From the power P_f dissipated by the freely decelerating tribometer, we obtain the dissipative contribution due to (AD + MF) that we take to be constant in all our measurements since all the tests are performed under the same conditions. P_f increases with increasing ω due to the AD term, that is proportional to ω^2. To obtain the power dissipation due to the friction between the slider and snow (P_{fri}) we determine the total dissipated power P in a test performed with the running slider and we subtract the contribution of P_f

$$F_{fri} = -\frac{P - P_f}{v} = -\frac{P_{fri}}{v} \tag{3}$$

We obtain the frictional force F_{fri} between the slider and snow by Eq.3, where $v = r\omega$ is the average linear sliding velocity of the slider placed at radial distance r from the rotation center. The friction coefficient μ between the sample and snow is given by

$$\mu = \frac{F_{fri}}{F_n} \tag{4}$$

where $F_n = mg$ is the normal force perpendicular to the snow track, g is the standard gravity acceleration and $m = 0.692$ *kg* is the sum of the masses of the weight, the steel bar and the sample holder acting on the slider.

2.2. Contact angle measurements

Water contact angles (CA) were measured at room temperature with a sessile drop system using 3 μL of distilled water. Optical contact angle measurements were carried out using an OCA 20 instrument (Dataphysics Co., Germany), equipped with a CCD photo-camera and with a 500 μL Hamilton syringe to dispense droplets of the testing liquid. Every CA value is the average out of the CAs obtained at 5 different positions (at the center and near the four corners) on the surface of the sample.

For all samples CA measurements were performed thirty days after the surface treatments. During this time the samples were stored in the laboratory in closed, but not sealed envelopes. Hi-fs and Hi-ps samples were further protected by a polymeric film. One week after performing the tribometer tests, we repeated CA measurements.

3. Results and Discussion

In Fig. 3 we display representative SEM surface micrographs of the LIPSS obtained after different laser irradiation procedures of the four samples taken before testing the samples on the tribometer.

We analyzed the SEM images of Fig. 3 by performing a 2D-FFT (bi-dimensional Fast Fourier Transform) analysis. We calculated the spatial period of the LIPSS as the reciprocal of the distance between the center and the shade of the pattern in the 2D-FFT image. In Table 2 we report the result for the LSFL. These correspond to the surface patterns most evident to the naked eye, whereas inside the concavities of the LSFL thinner ripples nicely aligned with each other (HSFL) are also visible (Fig. 3e). HSFL's are clearly oriented normally to LSFL's.

From Table 2, looking at LSFL the spatial periodicity between the parallel ripples of the four samples is almost the same. This is expected since we adopted practically the same laser wavelength (1030 nm; 1064 nm) for all surface treatments. Some of the ripples are subdivided into sub-ripples, the spacing of which is almost half of the spacing between the main ripples [26]. In all the samples we observe also bifurcations that occur when a ripple splits into two [22,27]. These features are most evident for the three ps laser treated samples (Fig. 3b,c,d). In the case of ps-treated samples the ripples are continuous, while for the fs-treated sample some of the ripples are interrupted. We find also spherical nanoparticles (visile in Fig. 3) with a maximum size of 100 nm [26,27].

In the regions where pronounced LSFL were formed, they were always accompanied by HSFL. We did not investigate how HSFL, that are present also after prolonged tribometer testing (see Fig. 7b, d), impact on the gliding behavior of AISI 301. Thus, we cannot separate the effect on friction coefficient of HSFL alone.

In Fig. 4 we display the average CA value of each sample, measured

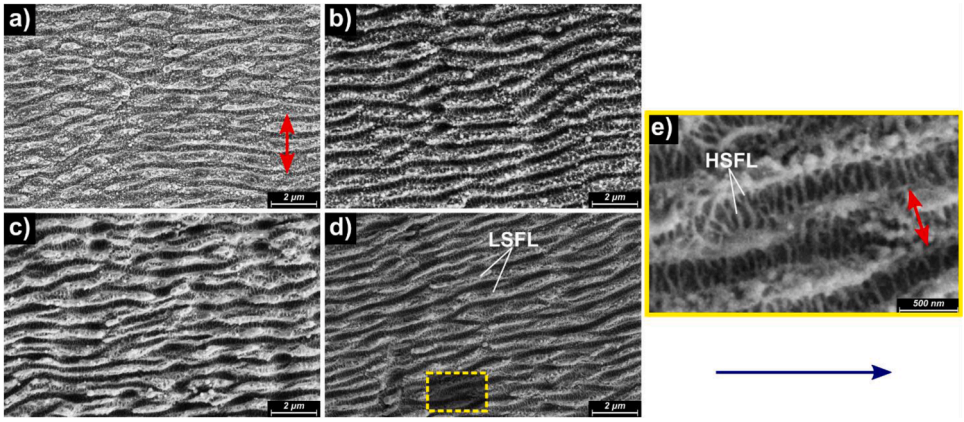

Figure 3. SEM micrographs of LIPSS on AISI 301 surfaces upon different laser irradiations. The red arrow represents the light polarization direction. a) Hi-fs, b) Hi-ps, c) LP-ps1 and d) LP-ps2. e) Magnification of the inset of panel d) showing the HSFL details. For all panels the blue arrow represents the sliding direction of the sample.

Table 2
Periodicity of LIPSS for the different samples.

sample	LSFL (nm)	st. dev. (nm)
Hi-fs	749	61
Hi-ps	722	153
LP-ps1	739	129
LP-ps2	777	102

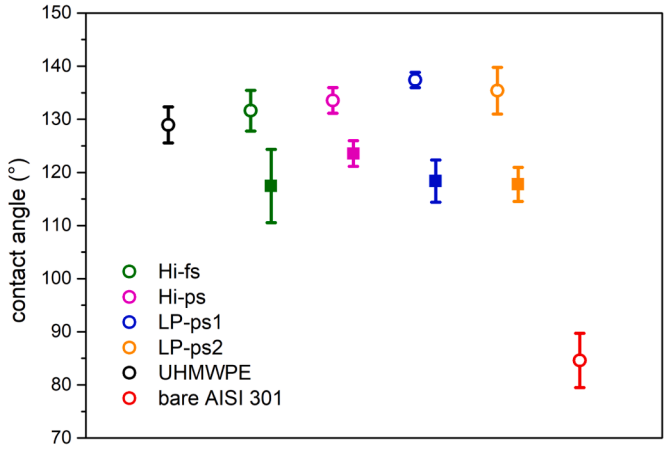

Figure 4. Average CA values of the considered samples before (dots) and after (squares) performing the tribometer tests.

before performing the tribometer tests (dots). Compared to bare AISI 301, all the samples show a marked increase of CA with water. From the figure we notice that the CA values of the LIPSS-treated samples are slightly higher than the CA of UHMWPE, and that CA data show a modest dispersion. The CA values we measured agree with the asymptotic, long-time values reported for aged AISI 301 [28].

3.1. Friction coefficient

The friction between a solid surface and ice is a classical problem in tribology. We summarized the friction between UHMWPE and snow with specific reference to the relevant parameters for alpine skiing [13]. A systematic analysis of the gliding performance on snow of several surface patterned polymeric materials, including UHMWPE, was performed [29] investigating the effect both of the base roughness (in the range 0.05 to 10 μm) and of pattern directionality. Above a threshold roughness (1 μm) the friction coefficient is minimum when the gliding direction is parallel to the pattern orientation. With a specific interest to improve ski edges, the friction of C60 was investigated with a linear snow tribometer, at progressively increasing velocities between 0.1 and 12 ms^{-1}. Again, roughened surfaces showed better performance with respect to flat ones [30]. Curiously, this is contrary to the practice of top-level skimen, who point at making the surfaces of ski edges as smooth as possible.

In Fig. 5a we report the measured values of the friction coefficient (μ) for all our samples, taken over the velocity range 0.8-7.2 ms^{-1}. Remarkably (see sect. 2, experimental) during the measurements of the friction coefficient the temperature of the snow track increased progressively from –10°C to –5°C/–4°C. This means that μ depends both on the sliding velocity and on the snow temperature. Our choice to avoid using a climatic chamber in these experiments is dictated by the aim to simulate the conditions occurring on a slope where the temperature at the higher altitude starting point is nearly always (an exception is during a snowfall) considerably lower than at the slope arrival, at lower altitude. Since the load on the tribometer slider is adjusted to reproduce the same pressure exerted on the skis by a skier with a mass of 80 kg, we expect that pressure induces the formation of a localized, transient quasi-melted thin snow layer, such as is believed to occur when skiing (except at very low temperature, below -20°C, where dry friction occurs, resulting in consistently reduced gliding velocity). The thickness of such a thin layer depends on the snow temperature, since the pressure exerted by the slider on the snow is constant. Along all our measurements we never observed any signature of formation of a liquefied surface layer after the slider stopped, nor a macroscopic modification of snow morphology, as associated to the average snow grain size and a change of the optical reflectivity of the snow track "lane" along which the slider travelled.

In principle samples with different μ values could give rise to different heating of the snow track with two consequences: a surface layer of snow melts and friction coefficients of differently treated steels are not comparable to each other and to UHMWPE. To solve the above difficulties, we consider the two materials with the largest μ value difference, namely bare AISI 301 and UHMWPE and the most demanding test conditions. At the highest sliding speed (10 ms^{-1}) the time required by the slider to travel a "lane" sector 5.1 cm long, corresponding to its projected length on the track, is $t_1 = 4 \times 10^{-3}$ s. Using the relation [31]

$$\Delta T = \frac{2\mu F_n}{A\lambda}\left(\frac{\alpha t}{\pi}\right)^{\frac{1}{2}} \quad (5)$$

where α is the thermal diffusivity of ice (9.3×10^{-7} m^2s^{-1}; a reasonable approximation for the highly compacted snow we use), A is the slider

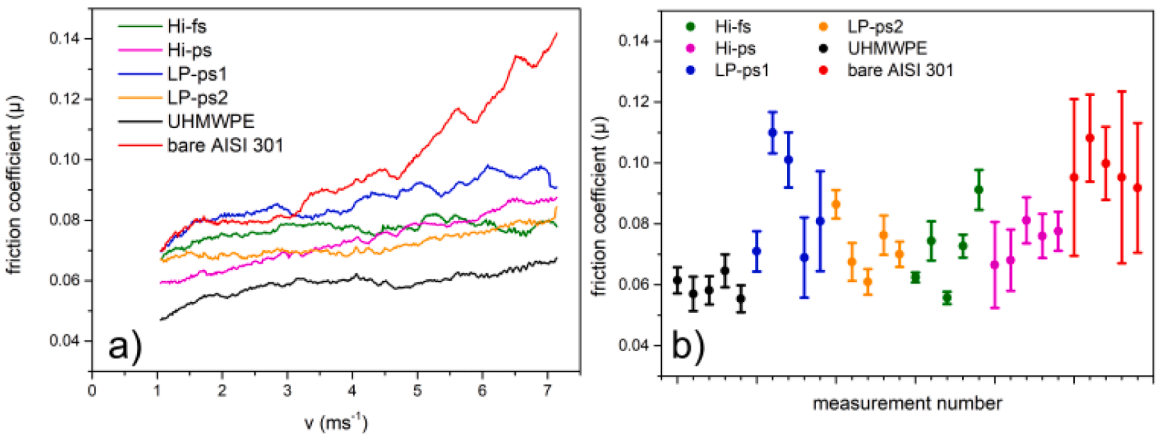

Figure 5. a) Friction coefficient μ as a function of sliding velocity *v* for the considered samples. Each curve refers to the average out of the five different measurements reported in b). In every measurement μ values are taken at discrete steps of $1 \bullet 10^{-2}$ ms^{-1}. b) Average μ values (closed circles) and standard deviations for the five single measurements performed on each sample over the velocity range 0.8 - 7.2 ms^{-1}.

surface and λ is the thermal conductivity of ice (1.8 $Wm^{-1}K^{-1}$), the increase of snow surface temperature is $\Delta T = +0.13°C$ for bare AISI (μ = 0.1) and $\Delta T = +0.06°C$ for UHMWPE (μ = 0.05).

With the hypothesis that *all* the produced thermal energy is dissipated by conduction in the snow, by a simple thermodynamic balance the thickness of the heated snow layer is 56 μm.

At the speed of 10 ms^{-1} the time needed by the track to travel one lap before the subsequent contact of the slider surface with the same above considered "lane" sector is $t_2 = 8.1 \times 10^{-2}$ s. Again adopting a conservative approach, after time t_2, neglecting thermal energy transmission channels other than conduction, the residual temperature increase of the "lane" sector surface, obtained by Fourier equation, is $\Delta T_{1,\ steel} = +7 \times 10^{-3}°C$ (bare AISI 301) and $\Delta T_{1,PE} = +\ 4 \times 10^{-3}°C$ (UHMWPE).

To bring to rest the slider the higher necessary number of laps (UHMWPE, lower μ value) is N = 482; with our conservative approach we neglect the increasingly reduced heating with progressively lowering slider speed and we sum N residual temperature increases ΔT_1, obtaining $\Delta T_{tot} = +3.37°C$ (bare AISI 301) and $\Delta T_{tot} = +1.93°C$ (UHMWPE). Taking as the initial snow temperature –10°C (although the high-speed tests were conducted from –15°C) even in the most unfavorable case of bare AISI 301, snow track temperature remains far from melting. Since all the μ values for *treated* AISI 301 surfaces lie in between the two above considered extremes, snow track heating can be taken as irrelevant. Since snow temperature and water vapor absorption could only weakly affect the *absolute* μ values we obtain, it is meaningful to compare to each other the μ values of differently prepared surfaces gliding on snow of the same initial kind that evolves for the same time under the same mechanisms.

Throughout the investigated range of sliding velocities UHMWPE displays the minimum μ value that slightly increases with increasing sliding velocity. On the opposite side the μ value of bare AISI 301 almost doubles from 0.07 at 1 ms^{-1} to 0.14 at 7.2 ms^{-1}. With increasing sliding velocity LIPSS treated samples show μ trends similar to that of UHMWPE. We observed the best results for the Hi-ps and LP-ps2 samples with nearly halved friction coefficient value with respect to that of bare AISI 301.

In Fig. 5b, after *single* measurements performed on each sample over the velocity range 0.8 to 7.2 ms^{-1}, we display the obtained average μ values. The standard deviation of bare AISI 301 is the largest, corresponding to the consistent increase of μ values with increasing velocity. The data points for UHMWPE lie on the opposite side. The data trend of sample LP-ps1 is presently unexplained and it corresponds to the strong oscillation of μ values with velocity (Fig. 6).

The μ values after the slowing down tests from the highest sliding velocity are shown in Fig. 6. With a trend similar to what observed at

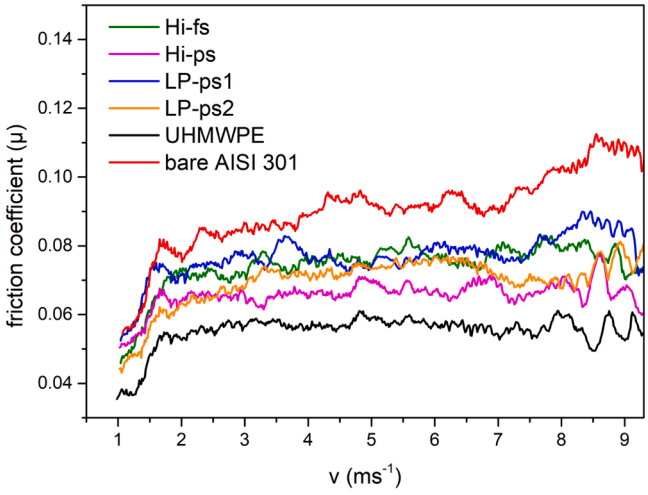

Figure 6. Friction coefficient μ as a function of sliding velocity *v* for the considered samples. Results of single measurements from the highest available sliding velocity.

low sliding velocities, the friction coefficient of bare AISI 301, for which the CA value is the lowest one (see Fig. 4) increases most with increasing sliding velocity *v*. The μ trends for laser treated samples, that show all comparable morphology and wettability (see Fig. 3), are comparable to each other: the μ values remain practically constant over the entire velocity range (see Figs. 5a; 6). The treatment Hi-ps corresponds to slightly lower μ values (Fig. 6), although still higher (by about 15%) than μ for UHMWPE. Overall, looking at the other treatments, the μ values are comparable to each other, and they are worse than the reference UHMWPE by about 30%.

3.2. *Durability of the LIPSS*

In Fig. 7 we show micrographs of the LIPSS of our samples, taken after several tribometer tests (including tests not discussed here), up to an estimated overall average distance of about 10 km travelled by each sample. The regularity of LIPSS is evident throughout the entire surfaces. Notice that HSFL are still visible (Fig. 7d). We observe the presence of localized small scratches (Fig. 7a) and a flattening of the ripples such as in Fig. 7b). Since there are no debris on the snow track, we assume that such scratches were caused by the repeated sliding against sharp asperities of ice I_h (hardness between 15 and 20 MPa at the

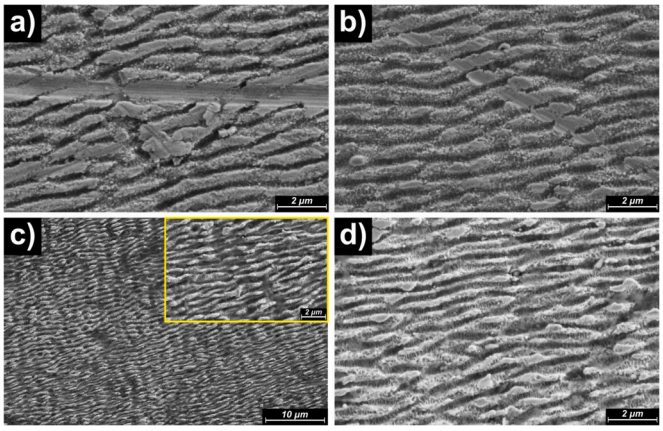

Figure 7. SEM micrographs after performing the tribometer tests of a) Hi-fs, b) Hi-ps, c) LP-ps1 and d) LP-ps2. The lower magnification of panel c) allows to appreciate the overall regularity of the surface pattern; in the inset, for comparison, the same surface magnification as for panels a), b), d) is provided.

explored temperatures [32]). We remark that, although counterintuitive, the same kind of shallow, thin scratches were occasionally observed on the surface of AISI 301 bare bases of full-size prototype skis used in mid-January, early morning, on slopes freshly prepared for international competitions with artificial snow, carefully checked to remove any debris accidentally present. Again, we are inclined to suppose that such scratches are caused by sharp, localized ice asperities, possibly remaining after artificial snow distribution and compaction on the slope.

We observed LIPSS surfaces after aging for 30 days in the laboratory at room temperature in non-controlled atmosphere. The initially iridescent surface darkened and resulted opaque due to hydrocarbon adsorption [28]. While the contaminant film was not removed both by standard polishing with acetone and ultrasonication, after repeated tribometer testing at the same conditions adopted for the above discussed clean samples, the measured friction coefficient values were comparable to those of fresh samples [25].

The average CA values measured on the sample surfaces of Fig. 7 are reported (squares) in Fig. 4. The decrease of CA of the laser treated surfaces from around 130° (before testing; see Fig. 4, dots) to around 120° marks the effect of prolonged sliding on a quite demanding kind of snow. Yet, the surface behavior of laser treated AISI 301 remains truly hydrophobic. We compared also with CA values for bare AISI 301 and UHMWPE, both *not* tested at the tribometer [25]. In the case of bare AISI 301, the comparison is justified by the above-mentioned behavior of the material, the surface of which remains unaltered after extensive field tests. As to UHMWPE, a grinded ski base keeps nearly unaltered the CA value after travelling large distances, even greater than the distance travelled by AISI 301 laser treated surfaces in the present tests (around 10 km). Obviously, the base has not to be damaged by accidental impact against debris, icy particles, dust or any other hard material during its sliding.

4. Conclusions

LIPSS, as produced on AISI 301 by four different ultra-fast laser treatments, were characterized via SEM observations and contact angle measurements. The observed hydrophobic behavior of the samples was compared to that of UHMWPE and bare AISI 301 surfaces. The friction coefficient of all laser-treated *unwaxed* surfaces gliding on compact snow, as tested with a dedicated tribometer over a range of medium and low velocities, was better than that of bare AISI 301, although still worse than that of UHMWPE, waxed state of the art. While all the treated surfaces showed similar friction behavior, the best performance was offered by Hi-ps and LP-ps2 samples. SEM pictures and contact angles, as measured on the samples after protracted tribometer testing, confirmed the durability of LIPSS. Overall, the friction behavior on compact snow at low and moderate sliding velocities of unwaxed laser treated AISI 301 surfaces results in satisfactory frictional behavior as compared to that of UHMWPE waxed state-of-the-art. As such, LIPSS treatment of AISI 301 appears suitable to be applied to full size skis for alpine skiing.

Acknowledgments

This research was performed in the frame of the activities of CRYOLAB (Politecnico di Milano).

We acknowledge Blossom Skis (Prata Camportaccio, SO, Italy), for the permission to quote confidential research results on modified carbon-based materials and on prototype skis performance.

We are grateful to Dr. C. Liberatore for laser treatments performed in the initial stage of this research, to Ing. J. Sládek for the help in preparation of laser irradiation setup at HiLASE Center and to Ing. G. Tajé for tribometer measurements at SWIS Lab Politecnico di Milano.

We acknowledge LaserPoint s.r.l. Vimodrone (MI, Italy) for the surface treatment of samples LP-ps1 and LP-ps2.

We are grateful to the Italian Winter Sports Federation (FISI) for having provided to us ambient data retrieved from 2021 World Cup competitions.

We acknowledge Prof. S. Turri and Dr. R. Suriano, ChIPLab, Dip. CMIC, Politecnico di Milano for contact angle measurements.

Participation of I.M. to this research was funded by the European Regional Development Fund and the state budget of the Czech Republic (project BIATRI, No. CZ.02.1.01/0.0/0.0/15003/0000445; project HiLASE CoE, No. CZ.02.1.01/0.0/0.0/15006/0000674; programs NPU I, project No. LO1602).

References

[1] L. Kuzmin, P. Carlsson, M. Tinnsten, The relationship between the type of machining of the ski running-surface and its wettability and capillary drag, Sports Technol. 3 (2010) 121–130, https://doi.org/10.1080/19346182.2010.538399.
[2] L. Canale, J. Comtet, A. Niguès, C. Cohen, C. Clanet, A. Siria, L. Bocquet, Nanorheology of Interfacial Water during Ice Gliding, Phys. Rev. X 9 (2019) 1–9, https://doi.org/10.1103/PhysRevX.9.041025.
[3] S.C. Colbeck, A Review of the Friction of Snow, J. Sports Sci. 12 (1994) 285–295, https://doi.org/10.1080/02640419408732174.
[4] A.-M. Kietzig, S.G. Hatzikiriakos, P. Englezos, Physics of ice friction, J. Appl. Phys. 107 (2010), 081101, https://doi.org/10.1063/1.3340792.
[5] A.-M. Kietzig, S.G. Hatzikiriakos, P. Englezos, Ice friction: The effects of surface roughness, structure, and hydrophobicity, J. Appl. Phys. 106 (2009), 024303, https://doi.org/10.1063/1.3173346.
[6] C. Sciancalepore, L. Gemini, L. Romoli, F. Bondioli, Study of the wettability behavior of stainless steel surfaces after ultrafast laser texturing, Surf. Coat. Technol. 352 (2018) 370–377, https://doi.org/10.1016/j.surfcoat.2018.08.030.
[7] A.I. Aguilar-Morales, S. Alamri, B. Voisiat, T. Kunze, A.F. Lasagni, The Role of the Surface Nano-Roughness on the Wettability Performance of Microstructured Metallic Surface Using Direct Laser Interference Patterning, Materials 12 (2019) 2737, https://doi.org/10.3390/ma12172737.
[8] A. Volpe, C. Gaudiuso, A. Ancona, Laser Fabrication of Anti-Icing Surfaces: A Review, Materials 13 (2020) 5692, https://doi.org/10.3390/ma13245692.
[9] M. Bonelli, A. Miotello, P.M. Ossi, A. Pessi, S. Gialanella, Laser irradiation-induced structural changes on graphite, Phys. Rev. B 59 (1999) 13513–13516, https://doi.org/10.1103/PhysRevB.59.13513.
[10] M. Bonelli, A.P. Fioravanti, A. Miotello, P.M. Ossi, Structural and mechanical properties of ta-C films grown by pulsed laser deposition, EPL 50 (2000) 501–506, https://doi.org/10.1209/epl/i2000-00297-5.
[11] D. Bolgiaghi, A. Miotello, P. Mosaner, P.M. Ossi, G. Radnoczi, Pulsed laser deposition of glass-like cluster assembled carbon films, Carbon 43 (2005) 2122–2127, https://doi.org/10.1016/j.carbon.2005.03.043.
[12] M. Bonelli, A. Miotello, P. Mosaner, C. Casiraghi, P.M. Ossi, Pulsed laser deposition of diamondlike carbon films on polycarbonate, Int. J. Appl. Phys. 93 (2003) 859–865, https://doi.org/10.1063/1.1530725.
[13] F. Ripamonti, V. Furlan, A.G. Demir, B. Previtali, M. Derai, F. Cheli, P.M. Ossi, Innovative metallic solutions for alpine ski bases, J. Vac. Sci. Technol. B. 36 (2018) 01A108, https://doi.org/10.1116/1.5002542.
[14] L. Claudi, New Metallic Solutions for Advanced Ski Bases, M.Sc. Thesis, Politecnico di Milano (unpublished), 2017.
[15] J. Bonse, S.V. Kirner, J. Krüger, Laser-Induced Periodic Surface Structures—A Scientific Evergreen, IEEE J. Sel. Top. Quantum Electron. 23 (2017) 1–15, https://doi.org/10.1109/JSTQE.2016.2614183.

[16] Z. Gousheng, P.M. Fauchet, A.E. Siegman, Growth of spontaneous periodic surface structures on solids during laser illumination, Phys. Rev. B 26 (1982) 5366–5381, https://doi.org/10.1103/PhysRevB.26.5366.
[17] J.E. Sipe, J.F. Young, J.S. Preston, H.M. vanDriel, Laser-induced periodic surface structures. I. Theory, Phys. Rev. B 27 (1983) 1141–1154, https://doi.org/10.1103/PhysRevB.27.1141.
[18] P. Sigmund, Theory of Sputtering. I. Sputtering Yield of Amorphous and Polycrystalline Targets, Phys. Rev. 184 (1969) 383–416, https://doi.org/10.1103/PhysRev.184.383.
[19] P. Sigmund, Particle penetration and radiation effects, Springer, Berlin, 2006.
[20] J. Reif, F. Costache, M. Bestehorn, Self-organized surface nanostructuring by femtosecond laser processing, in: J. Perriere, E. Millon, E. Fogarassy (Eds.), Recent advances in laser processing of materials, Elsevier, Amsterdam, 2006, pp. 275-289.
[21] M. Groenendijk, J. Meijer, Microstructuring using femtosecond pulsed laser ablation, J. Laser Appl. 18 (2006) 227–235, https://doi.org/10.2351/1.5060548.
[22] J. Bonse, R. Koter, M. Hartelt, D. Spaltmann, S. Pentzien, S. Höhm, A. Rosenfeld, J. Krüger, Tribological performance of femtosecond laser-induced periodic surface structures on titanium and a high toughness bearing steel, Appl. Surf. Sci. 336 (2015) 21–27, https://doi.org/10.1016/j.apsusc.2014.08.111.
[23] J.M. Liu, Simple technique for measurements of pulsed Gaussian-beam spot sizes, Opt. Lett. 7 (1982) 196–198, https://doi.org/10.1364/OL.7.000196.
[24] E. Maggiore, M. Tommasini, P.M. Ossi, Synthesis of natural-like snow by ultrasonic nebulization of water: Morphology and Raman characterization, Molecules 25 (2020) 4458, https://doi.org/10.3390/molecules25194458.
[25] G. Tajé, M.Sc. Thesis, Politecnico di Milano (unpublished), 2019.
[26] A.F. Pan, W.J. Wang, X.S. Mei, H.Z. Yang, X.F. Sun, The formation mechanism and evolution of ps-laser-induced high-spatial-frequency periodic surface structures on titanium, Appl. Phys. B 123 (2017) 1–11, https://doi.org/10.1007/s00340-016-6613-7.
[27] J. Reif, Basic Physics of Femtosecond Laser Ablation, in: A. Miotello, P.M. Ossi (Eds.), Laser-Surface Interaction for new materials production, Springer, Berlin, 2010, pp. 19–41 .
[28] G. Giannuzzi, C. Gaudiuso, R. Di Mundo, L. Mirenghi, F. Fraggelakis, R. Kling, P. M. Lugarà, A. Ancona, Short and long term surface chemistry and wetting behavior of stainless steel with 1D and 2D periodic structures induced by bursts of femtosecond laser pulses, Appl. Surf. Sci. 494 (2019) 1055–1065, https://doi.org/10.1016/j.apsusc.2019.07.126.
[29] J.L. Giesbrecht, P. Smith, T.A. Tervoort, Polymers on Snow: Toward Skiing Faster, J. Polym Sci Part B: Polym. Phys. 48 (2010) 1543–1551, https://doi.org/10.1002/polb.22033.
[30] S. Rohm, M. Hasler, C. Knoflach, J. van Putten, S.H. Unterberger, K. Schindelwig, R. Lackner, W. Nachbauer, Friction Between Steel and Snow in Dependence of the Steel Roughness, Tribol. Lett. 59 (2015) 1–8, https://doi.org/10.1007/s11249-015-0554-x.
[31] W. Nachbauer, P. Kaps, M. Hasler, M. Moessner, Friction between ski and snow, in: F. Braghin et al. (Eds.), The Engineering Approach to Winter Sports, Springer, New York, 2016, pp. 17–32.
[32] L. Poirier, E.P. Lozowski, R.I. Thompson, Ice hardness in winter sports, Cold. Reg. Sci. Technol. 67 (2011) 129–134, https://doi.org/10.1016/j.coldregions.2011.02.005.